National Transportation Safety Board

Office of Aviation Safety
Washington, D.C. 20594-2000
April 6, 2018

ATTACHMENT 7 to the METEOROLOGY FACTUAL REPORT
DCA17FA076

Boeing analysis of wind conditions at the accident aircraft's west ramp parking location on the accident day.

Submitted by: Mike Richards
NTSB, AS-30

Robert J. McIntosh
Director, Product Safety
Commercial Airplanes

The Boeing Company
P.O. Box 3707 MC 09-76
Seattle, WA 98124-2207

December 18, 2017
66-ZB-H200-ASI-19018

Lorenda Ward
Investigator In Charge
National Transportation Safety Board
490 L'Enfant Plaza, SW
Washington DC 20594-003

BOEING

Subject: Boeing Wind Model Analysis – Ameristar MD-83 N786TW Aborted Takeoff and Runway Overrun, Ypsilanti, Michigan, 08 March 2017

Dear Ms. Ward,

With regard to the subject event, the NTSB provided Boeing weather history data and data collected by the NTSB via drone. The weather history data represents the period of time Ameristar's MD-83 was parked in Ypsilanti prior to the aborted takeoff. The drone collected data provides information relative to the physical characteristics of structures and terrain in the vicinity of the ramp where Ameristar's MD-83 was parked in Ypsilanti. Boeing was asked to use the information provided by the NTSB to perform a wind model analysis to determine the wind conditions experienced by Ameristar's MD-83 while it was parked, prior to the subject event.

Please find attached to the E-mail providing this letter a report detailing the analysis performed by Boeing, at the request of the NTSB.

The information included with this correspondence is controlled under the US Export Administration Regulations (15 CFR Parts 300-799) and has been categorized as ECCN: 9E991.

Please feel free to contact us if you have any questions.

Best regards,

[redacted]

Robert J. McIntosh
Director, Product Safety

Enclosure: Boeing Wind Model Analysis – Ameristar MD-83 N786TW Aborted Takeoff and Runway Overrun, Ypsilanti, Michigan, 08 March 2017

Computational Fluid Dynamics Model Analysis of Winds Associated with the March 8, 2017 MD-83 Accident at KYIP

The Boeing Company

1. Methods

A high resolution, computational fluid dynamics (CFD) model wind simulation was performed utilizing the open source software OpenFoam (http://www.openfoam.com/). OpenFoam is a widely used CFD modeling software for both industry and university research applications. Appendix I includes a list of selected journal articles citing OpenFoam. In this study, a period of variable wind magnitudes, directions, and gusts was simulated over real-life mesh obstacles sampled by the National Transportation Safety Board's drone. Although the results of this simulation cannot be verified and error margins are unknown, it is believed that the results presented herein represent a plausible scenario of the complex wind flow pattern that is generated downwind of a hangar and other structures.

1.1 Mesh Preparation

Drone data mesh preparation for use in OpenFoam proved to be a significant effort before the wind simulation would stabilize and converge on a solution. Two separate drone mesh files, formatted as 3D model OBJ, were provided and shown in figure 1. One mesh represented the main hangar building structure and the other mesh represented surrounding terrain, trees, brush, vehicles, and other nearby structures.

The mesh files were combined and further processed using the open source software Blender (https://www.blender.org/). Several initial attempts were made to combine mesh files and import into the CFD model, but they all resulted in model instability. The following factors were found to play a key role in model stability and convergence with regards to mesh preparation:

- Non-manifold edges: The final combined mesh had to be "watertight" with essentially no holes (non-manifold edges). After merging the two mesh files, holes were filled in manually using Blender.
- Internal face skewness: the watertight combined mesh file was further processed upon importing in to the OpenFoam model using the utility SnappyHexMesh. It was found that setting "maxInternalSkewness=4" under meshQualityControls allowed for model stability.

The final mesh used for the CFD model wind simulation (Figure 2) is a blend of the combined drone mesh data inserted into a 500 X 500 m flat plane. For model stability, it was found that a flat, smooth plane was necessary along the model boundaries. Also, due to computational limitations, a subset of the

terrain data was used. Finally, an MD-83 model provided by Boeing was positioned in the mesh based on information provided by the NTSB.

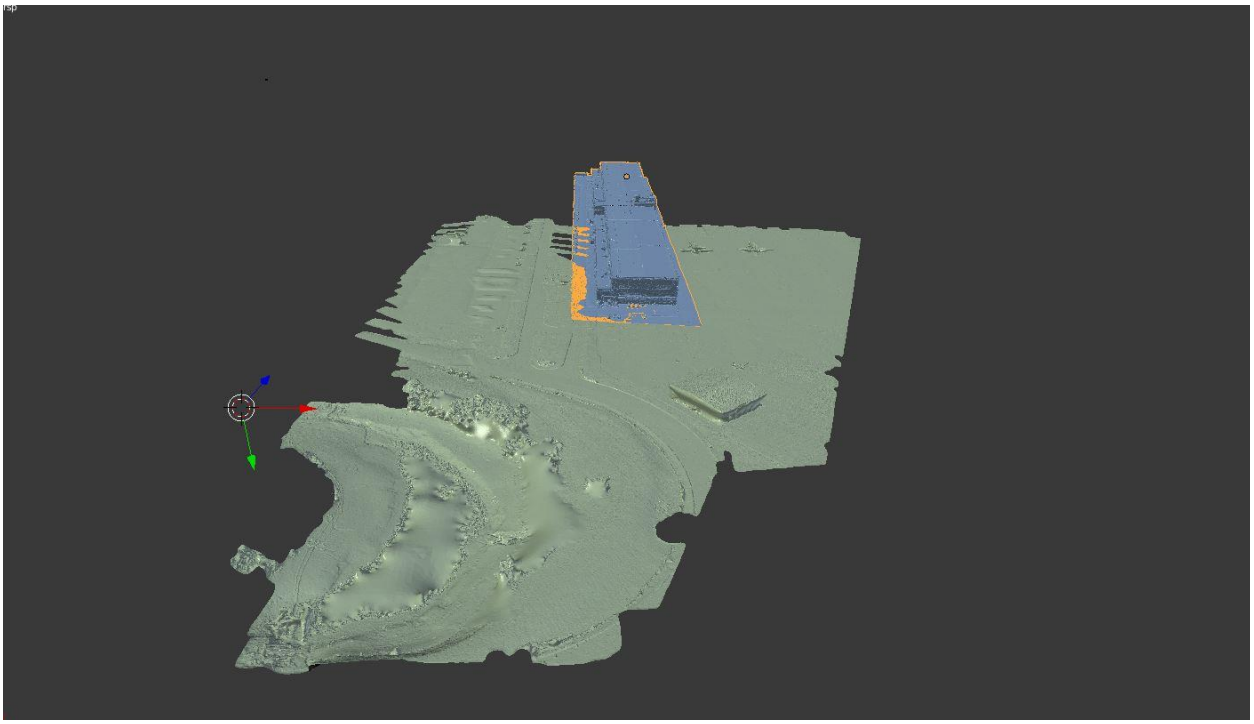

Figure 1.

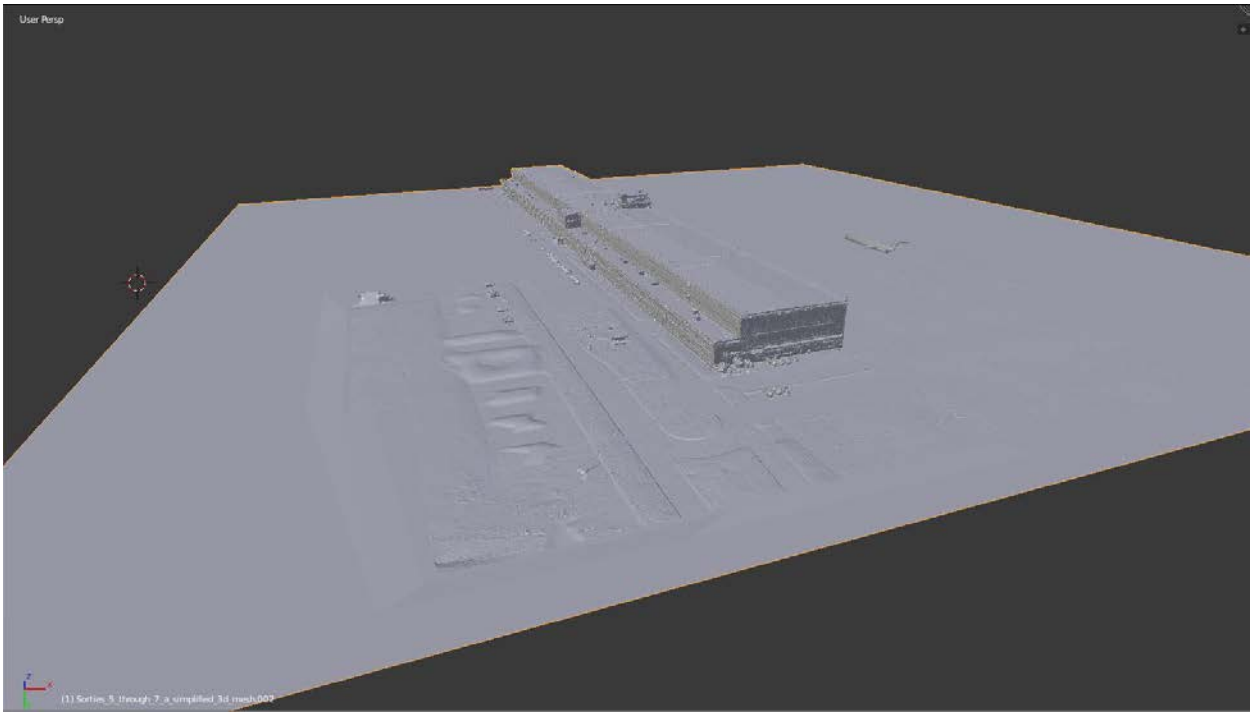

Figure 2.

1.2 CFD Model Numerical Solver / Scheme Details

The OpenFoam solver "buoyantPimpleFoam" was chosen for the CFD wind model simulation. The buoyantPimpleFoam solver is a transient solver for buoyant, turbulent flow of compressible fluids. Although the wind in this application is considered an incompressible fluid due to relatively low magnitude flow, this solver was used to capture small scale temperature and density driven flow.

The initial time step was set to deltaT=0.0005 sec with an automatic time step adjustment based on a maximum Courant number[1] set to 1.

Numerical schemes used:

- Euler for d/dt
- Gauss linear for gradients and divergence
- Gauss linear corrected for Laplacian terms

Solutions were solved using the PCG/PBiCG solver (preconditioned (bi-)conjugate gradient) with the DIC/DILU preconditioner (diagonal incomplete-Cholesky) along with residual control for U and p_rgh.

1.3 CFD Model Initial / Boundary Conditions

Shown in figure 3 is the model domain configuration. Moving along the **y-**axis in a positive direction is a north-bound heading (negative **y** is south) and along the **x**-axis in a positive direction is an east-bound heading (negative **x** is west). The **z**-axis is normal (perpendicular) to the ground surface plane and upward is in the positive **z** direction. Model winds will be referred to in vector notation where **U** is the 3-dimensional wind vector, which can be broken down into components (**u**,**v**,**w**) that flow along the **x**,**y**, and **z** directions respectively. Wind direction will be referred to in standard meteorological form where 0 degrees is wind coming from true north.

The model domain is a 500 X 500 X 100 m box with its west wall being the inlet, east wall being the outlet, and cyclic (period) boundary conditions for the north and south walls.
Cyclic conditions were implemented on the north/south walls to allow for wind components in the **v** direction to pass through without disrupting the pressure field and this also allowed for turbulence to build up over time.

[1] The Courant number is a measure of how much information traverses a computational grid cell in a given time-step. A Courant number <= 1 means that information will only propagate one grid cell per time step to insure proper numerical solutions.

The wind field **U** was initialized at the inlet to vary with time. Wind direction varied from roughly 240 to 260 degrees at magnitudes of 37-40 kt with gusts to 55 kt (table 1). In particular, this study focuses on the ASOS wind observations from March 8, 2017 from 11:37-11:39 EST (Appendix II). A no-slip condition was applied to the ceiling, partial slip (0.998) was applied to the building/terrain, and the "pressureInletOutletVelocity" conditions was used at the outlet.

Time (sec)	Direction (deg)	Speed (m/s)	Speed (kt)
0	248	5.4	10.5
10	247	11.5	22
20	261	19.2	37
30	255	21	40
35	261	28	55
38	257	20	39
42	246	23	45

Table 1. Model inlet wind.

Temperature (T_0) at the inlet just above the surface was prescribed to be 279 Kelvin (43F). The observed temperature reported by ASOS during the time of interest ranged from 276-283 Kelvin (38F-50F). Terrain and buildings were set to be 1-2 degrees K greater than the ambient air temperature.

Pressure (P_0) was set to 1013 mb near the surface for the internal field. The observed pressure reported by ASOS during the time of interest ranged from 1013-1010 mb. The Inlet pressure boundary condition was set to "zero gradient" and the outlet pressure boundary condition was set to "totalPressure".

A nested grid structured was used and the resolution varied from 10 m down to 0.625 m, which is shown in figure 4.

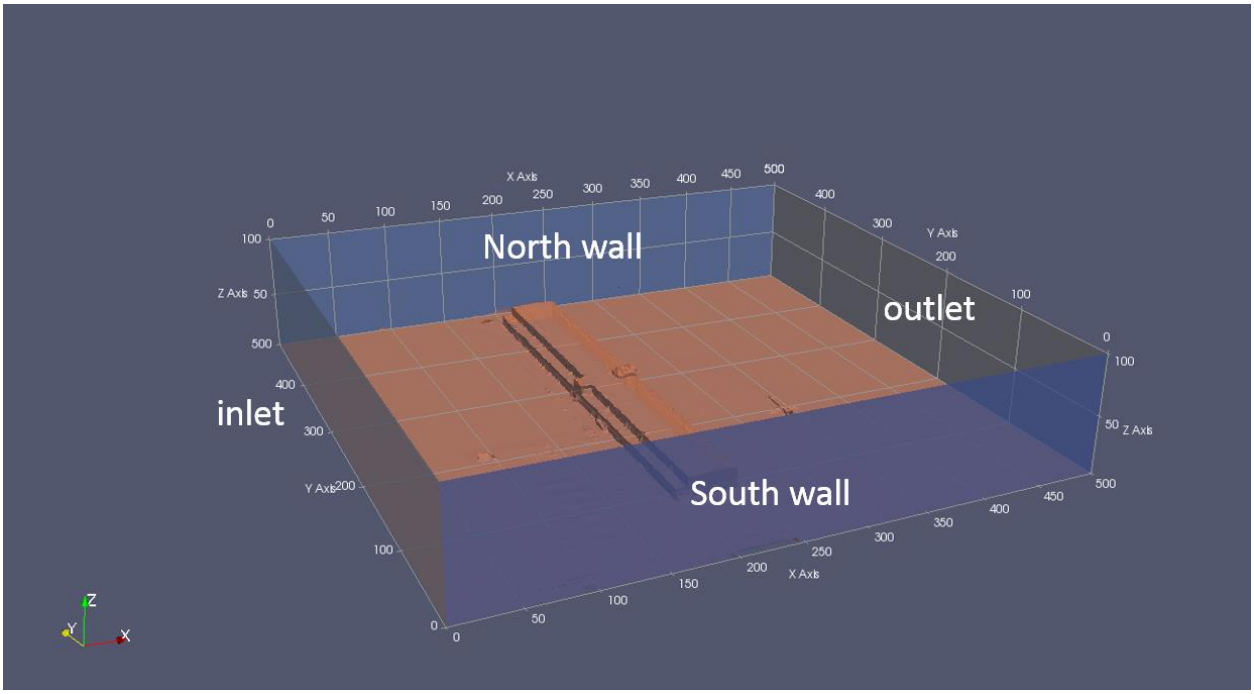

Figure 3.

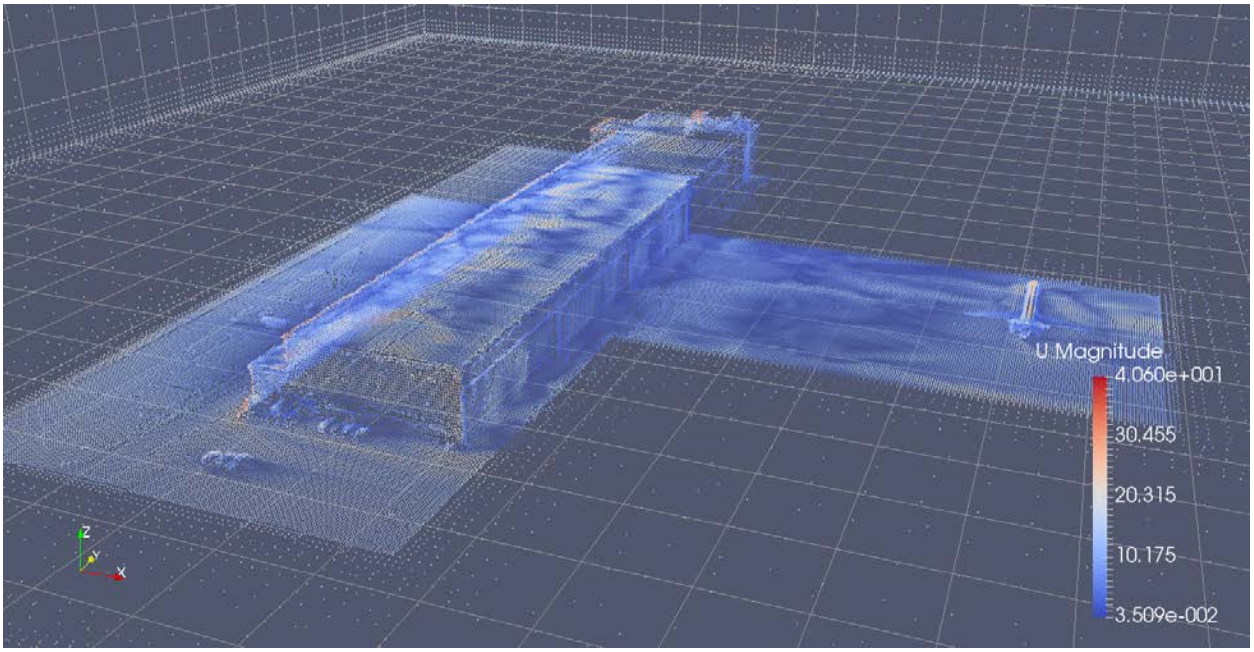

Figure 4.

Turbulence was modeled using a model that is a hybrid combination of the Reynolds-averaged Navier–Stokes (RANS) model and Large-Scale Eddy Simulation (LES) model. In particular, the Spalart Allmaras Improved Delayed Detached Eddy Simulation (IDDES) turbulence model was used:

> Shur, M. L., Spalart, P. R., Strelets, M. K., & Travin, A. K. (2008).
> A hybrid RANS-LES approach with delayed-DES and wall-modelled LES
> Capabilities. International Journal of Heat and Fluid Flow, 29(6), 1638-1649.

This particular turbulence model was selected after the computational cost of using a pure Large-Scale Eddy Simulation (LES) was found to be limiting in nature with the given resources and the much less computational costing RANS turbulence model was not appropriate since it was developed for steady-state, time-averaged simulations. Therefore, a version of the detached eddy simulation (DES) was chosen. A detached eddy simulation model is a modification of a RANS model in which the model switches to a subgrid scale formulation in regions fine enough for LES calculations. Regions near solid boundaries and where the turbulent length scale is less than the maximum grid dimension are assigned the RANS mode of solution. As the turbulent length scale exceeds the grid dimension, the regions are solved using the LES mode. Therefore, the grid resolution is not as demanding as pure LES, which considerably cuts down the cost of the computation.

1.4 Validity of Using ASOS Measured Wind for Model Inlet

A post model simulation analysis was performed to verify that the prescribed winds in the simulation can be correlated to the observed winds on the field. A lower resolution simulation was performed with an expanded domain to include the ASOS location to the east and structures to the west (upwind) of the hangar area (Figure 5). The ASOS location was probed at 10m above the surface plane and a 2-minute wind speed average was calculated. The same was done at 10m above the surface to the west of the hangar near the inlet of the high resolution model simulation (Hangar Ref in Figure 5). For this particular simulation, the average 2-minute wind magnitude at the ASOS location was 22.5 m/s (43.7 kt) and the average 2-minute wind magnitude at the hangar reference location was 22.0 m/s (42.8 kt). The hangar reference point wind magnitude was 98% of the ASOS location. This slightly lower wind magnitude can be explained by the up-stream building obstacles and river with trees in relative close proximity compared to the large fetch of open field up-stream of the ASOS location. From this analysis, it appears using the ASOS observed wind to initialize the simulation is valid.

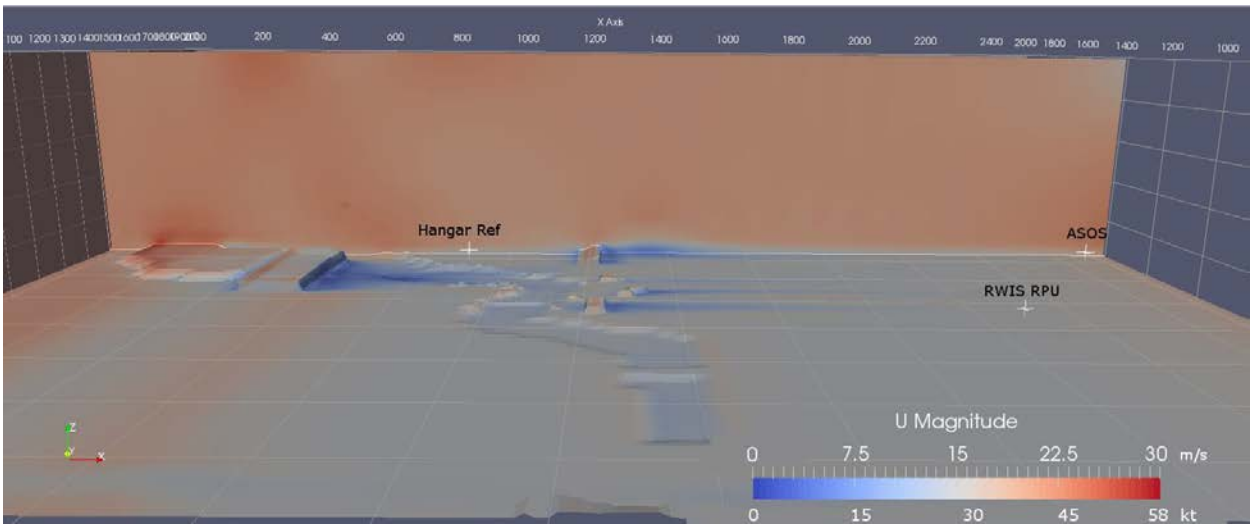

Figure 5.

2. Results

The model inlet wind magnitude was steadily increased to 20 m/s (39 kt) during the first 20 seconds of the simulation to avoid model induced pressure oscillations. At 15 seconds, winds were near 15 m/s (29 kt) from 255 degrees and the hangar's downstream wind pattern became established (Figure 6). The "**U** Magnitude" shown represents the total magnitude of the wind's (**u**,**v**,**w**) vector components where:

$$\mathbf{U}\ \text{Magnitude} = (\mathbf{u}^2 + \mathbf{v}^2 + \mathbf{w}^2)^{1/2}$$

A vertical vortex developed just downwind of hangar's southeastern corner due to wind shear induced by the obstruction in the wind flow. As flow wrapped around the southern part of the hangar, it acquired a southerly component, which appeared to contribute to the development of convergent zone where south-southwesterly flow met the westerly wind flow. Also, a shear induced horizontal vortex (directed south-north) developed just downstream of the hangar as strong flow sheared over the stagnant flow behind the building. At this point in the simulation, winds near the parked airplane were similar to the general ambient flow.

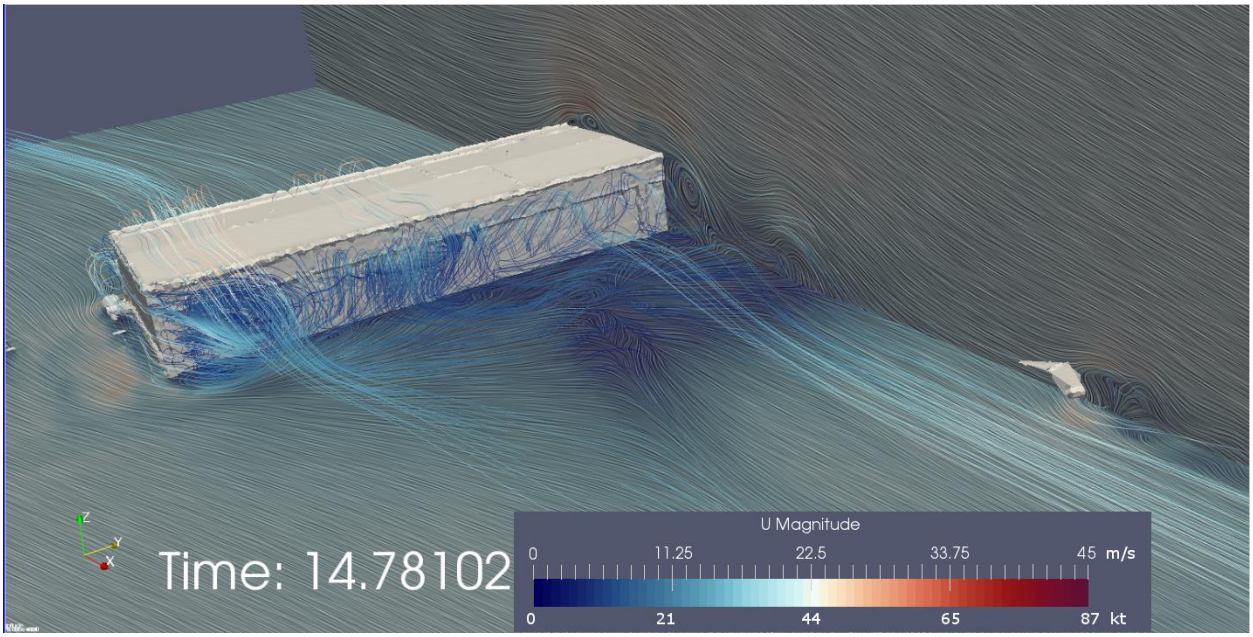

Figure 6.

By 27 seconds into the simulation, model inlet wind was steady-state and at 20 m/s (39 kt) from 255 degrees (figure 7). The vertical vortex appears to have combined with the horizontal vortex and quickly tilted 90 degrees conforming to the shape of the hangar. As winds wrapped around the corner and down from the roof, the convergent zone tightened up and moved northeastward closer to the airplane. This convergent zone appeared to play a role in breaking wave / turbulence generation near the airplane in time. The upward motion generated within the convergent zone disrupted the stronger wind flow just above hangar height causing brief pulses of strong wind to be transported downward. At this point in the simulation, the wind magnitude near the airplane was similar to the ambient flow, but slightly more turbulent.

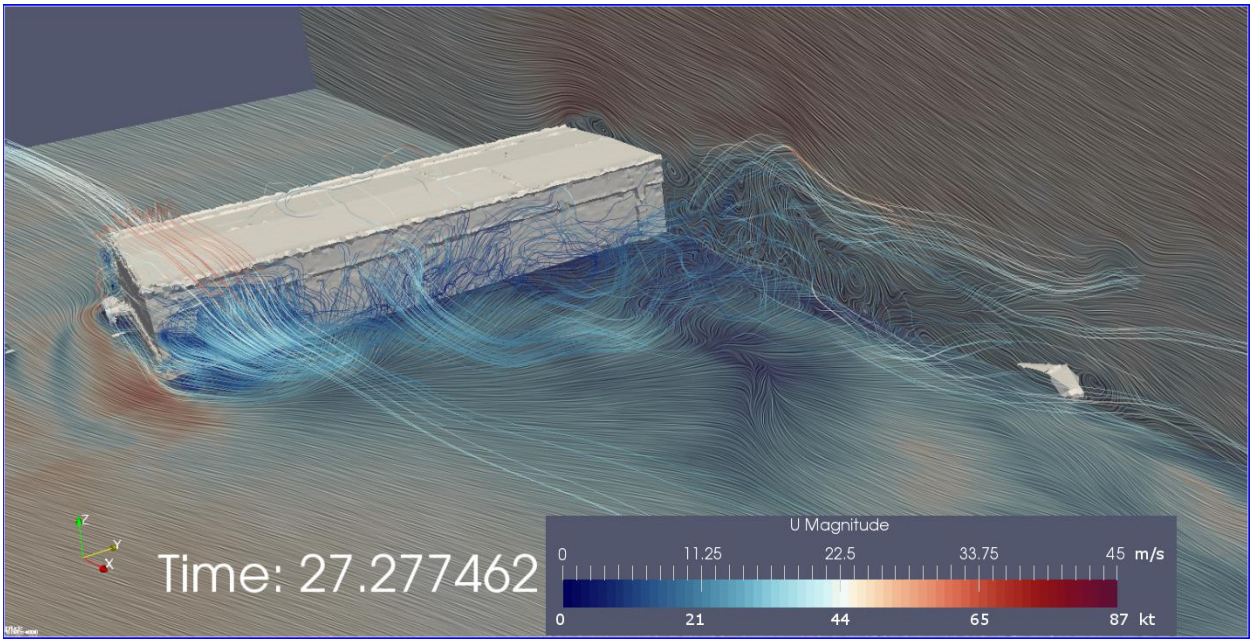

Figure 7.

A wind gust of 28 m/s (~55 kt) from 261 degrees, simulating observed ASOS gust conditions, was introduced into the simulation at 32 seconds and shown in figure 8. At that time, a small region of 30+ m/s (58+ kt) winds were brought down to ground level just downstream of the convergent zone. Winds near the aircraft were about 15 m/s (29 kt) at that time.

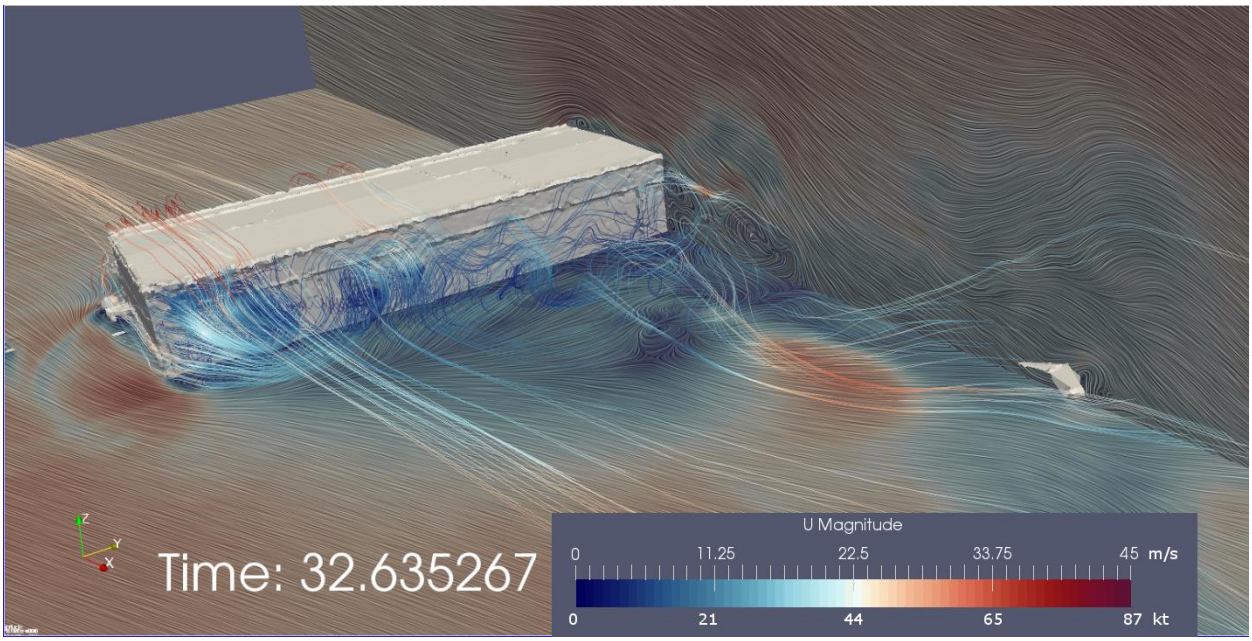

Figure 8.

At time=34 seconds, the small scale 30+ m/s (58+ kt) gust moves over the airplane (figure 9). This gust appears to be related to turbulence generated downstream of the hangar.

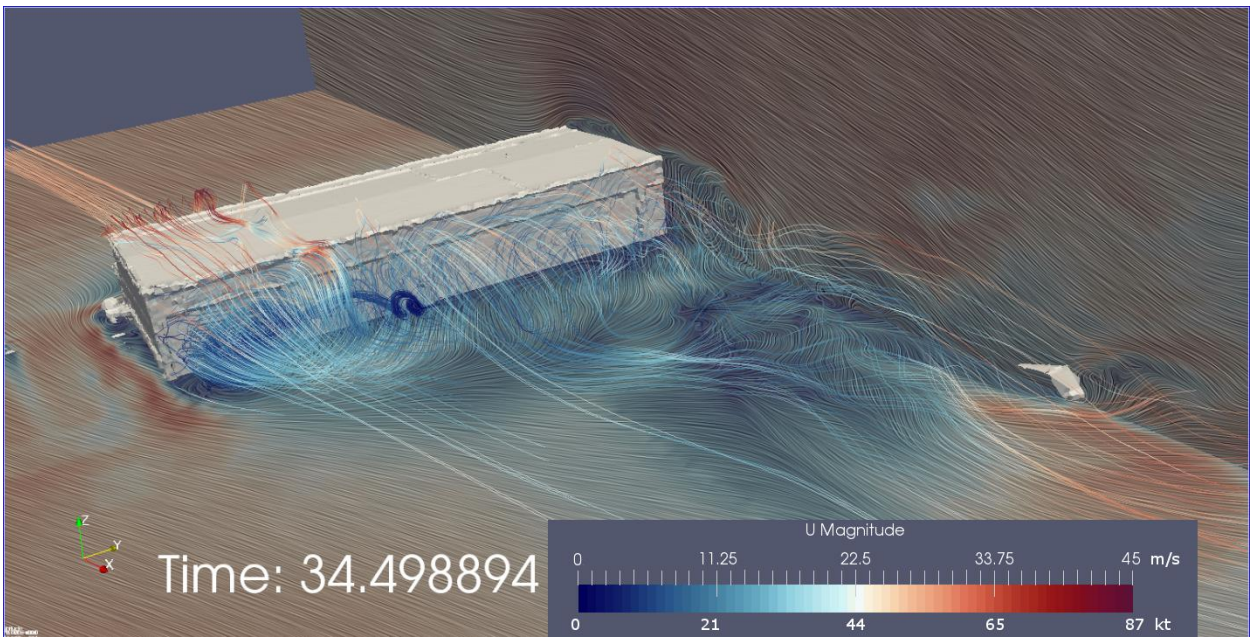

Figure 9.

The wind's vertical vector component **w** is plotted in a series and shown in figures 10-14. Small scale -15/+15 m/s (-29/+29 kt) **w** couplets were present and moving eastward with the turbulent gusts / waves that were being generated downstream of the hangar. These couplets had a wave length of about 30 meters and were moving approximately 10 m/s (19 kt).

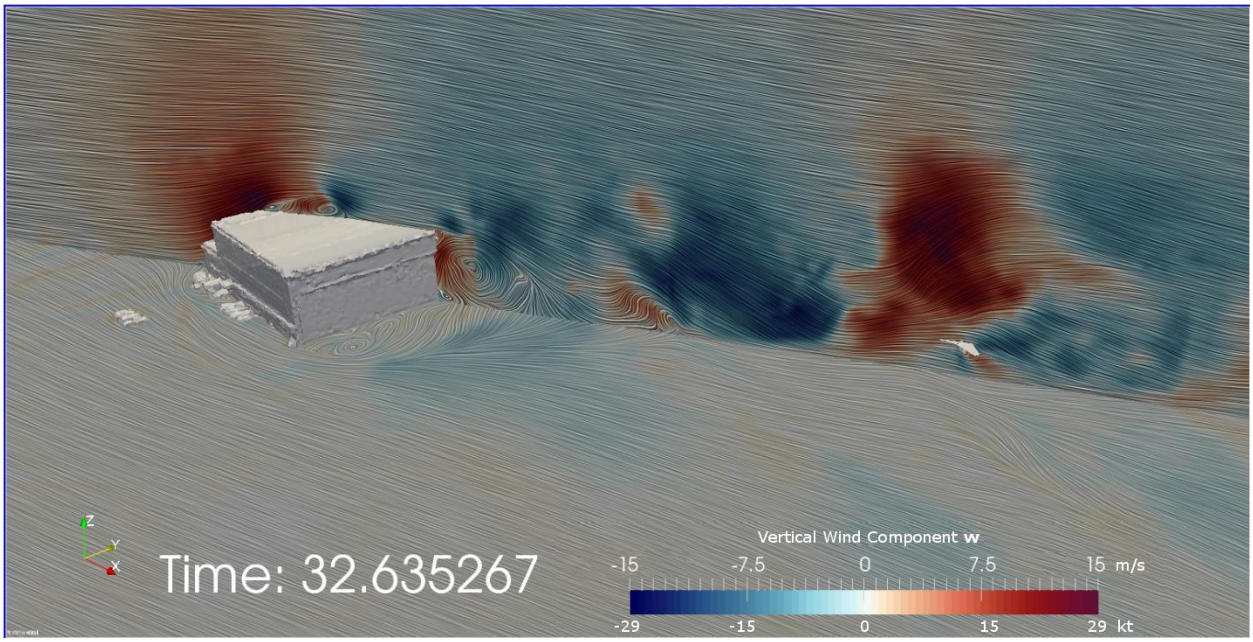

Figure 10.

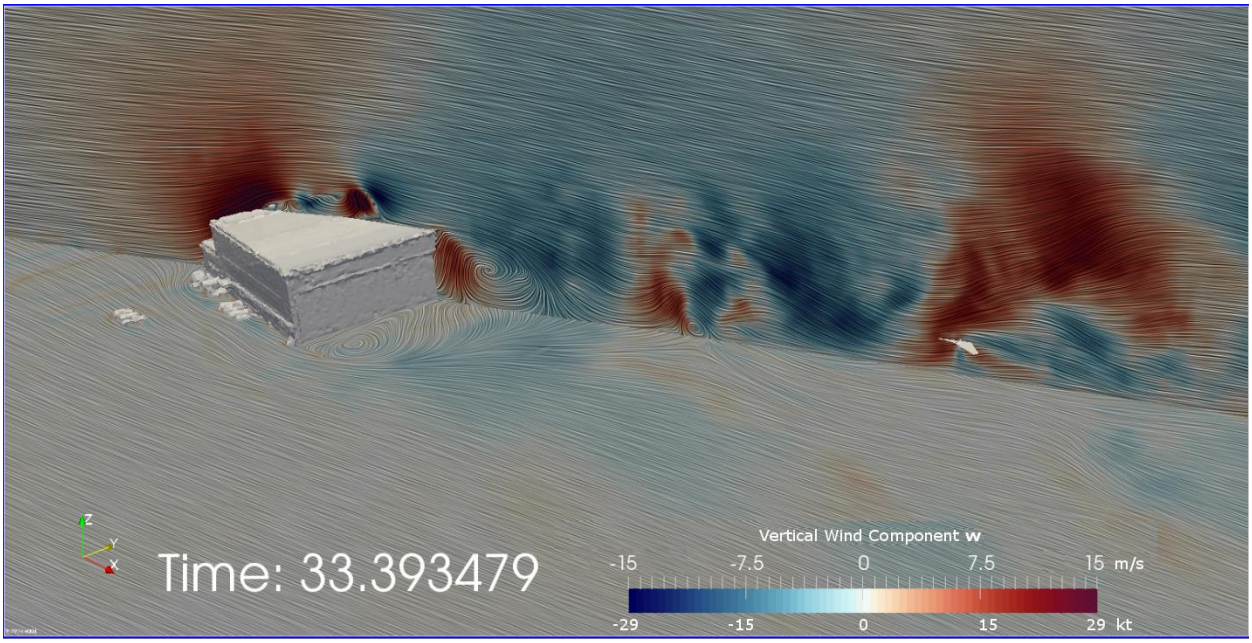

Figure 11.

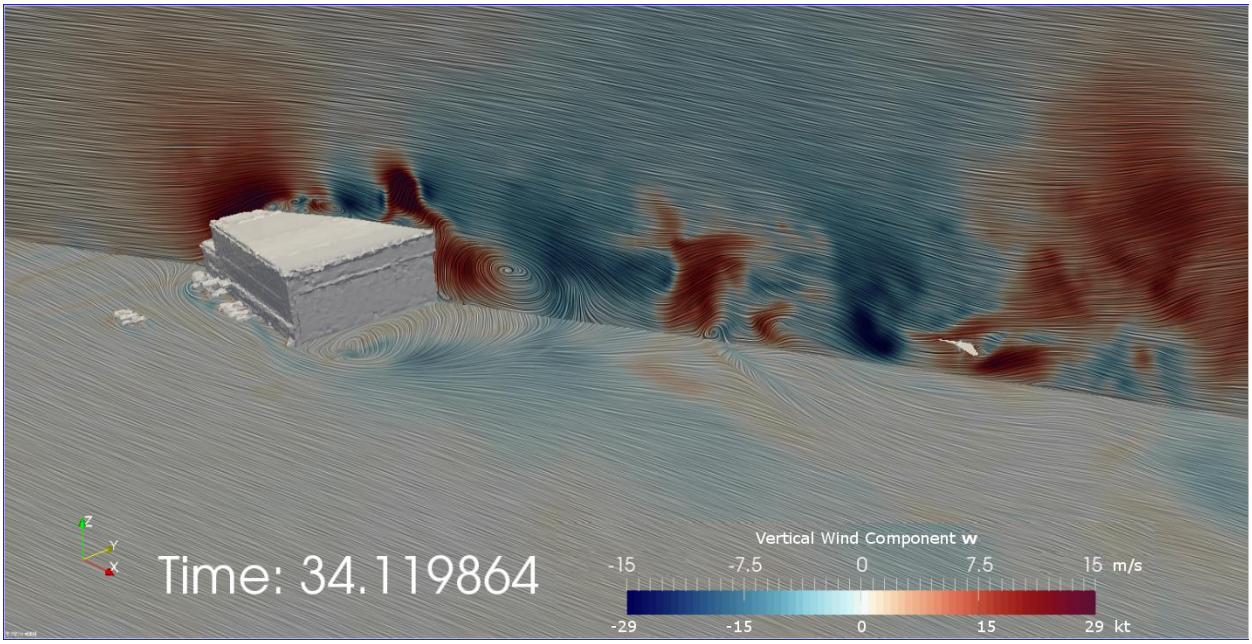

Figure 12.

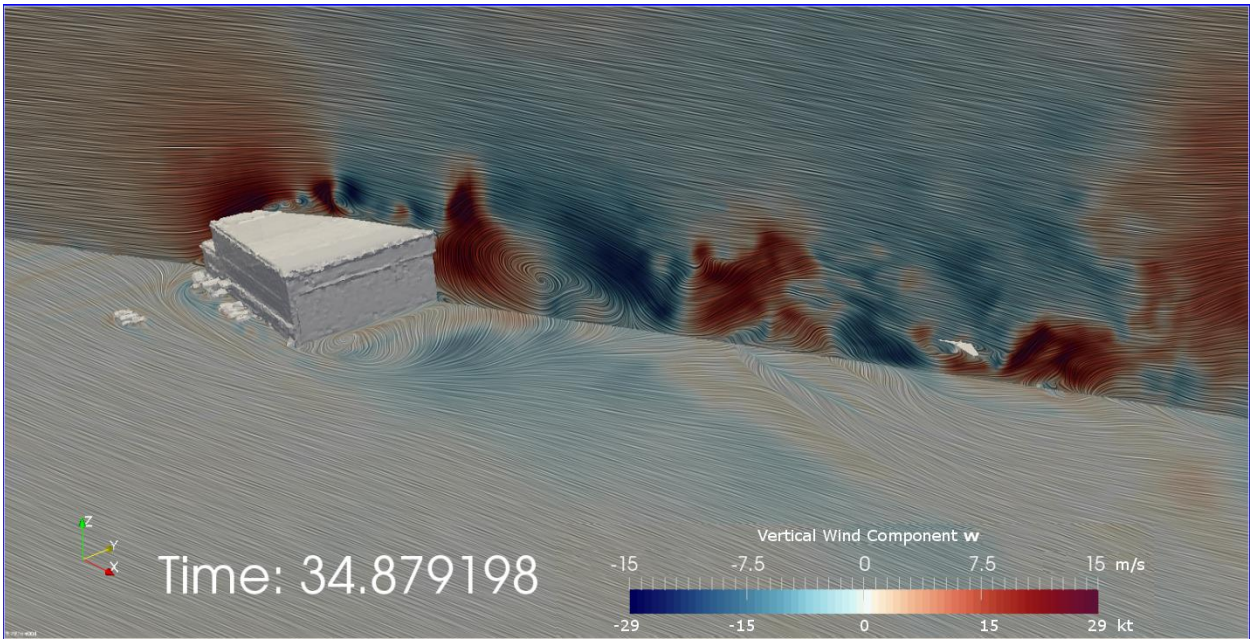

Figure 13.

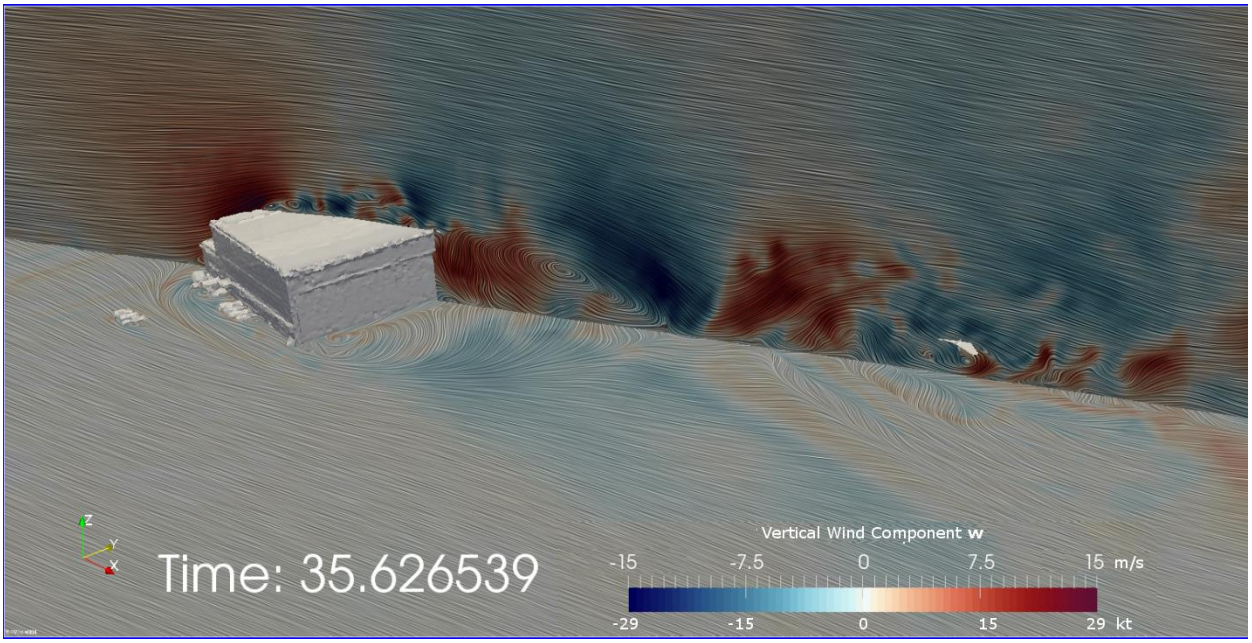

Figure 14.

A series of close-up viewpoint **U** and **w** are plotted in Figures 15-19.

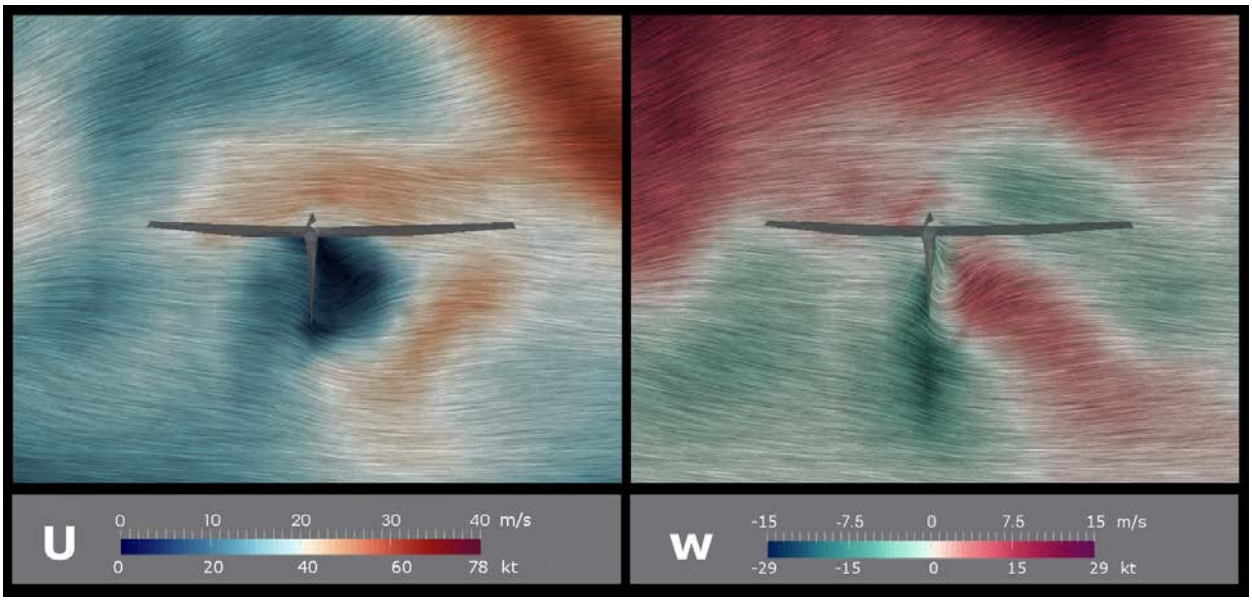

Figure 15. **U** and **w** for time = 32.6 sec.

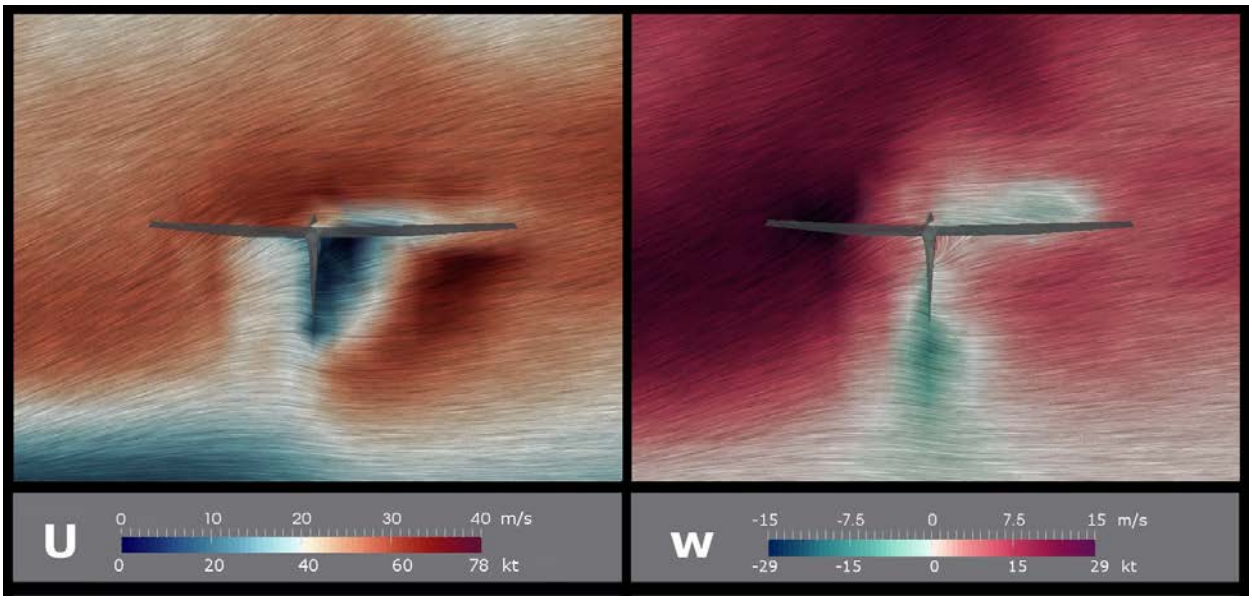

Figure 16. **U** and **w** for time = 33.4 sec.

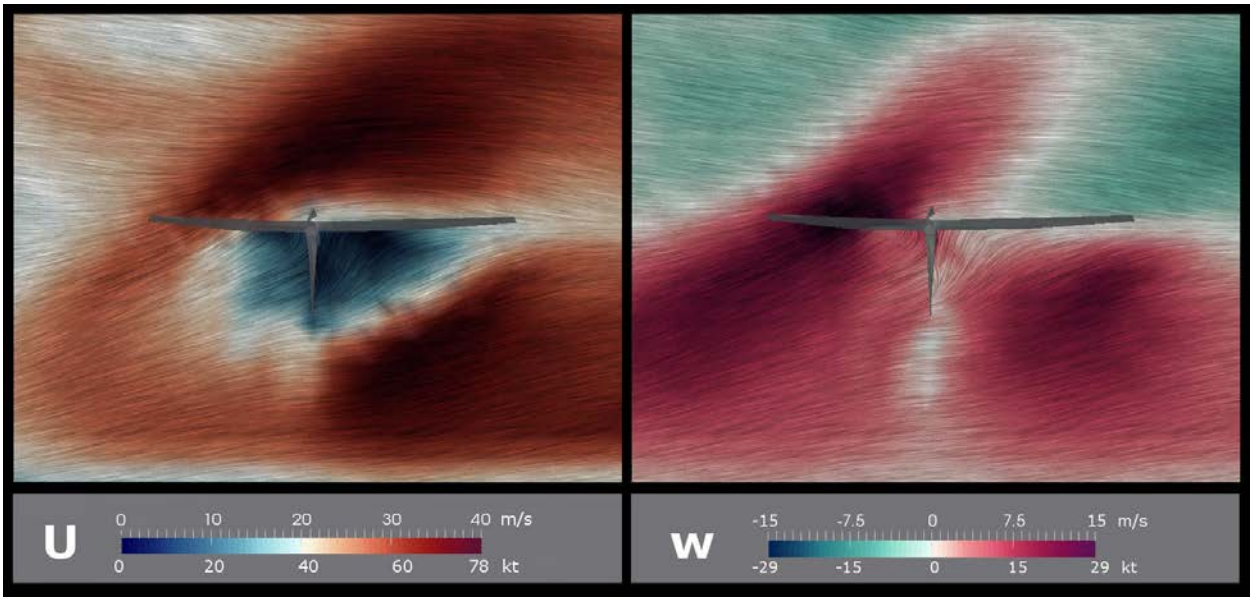

Figure 17. **U** and **w** for time = 34.1 sec.

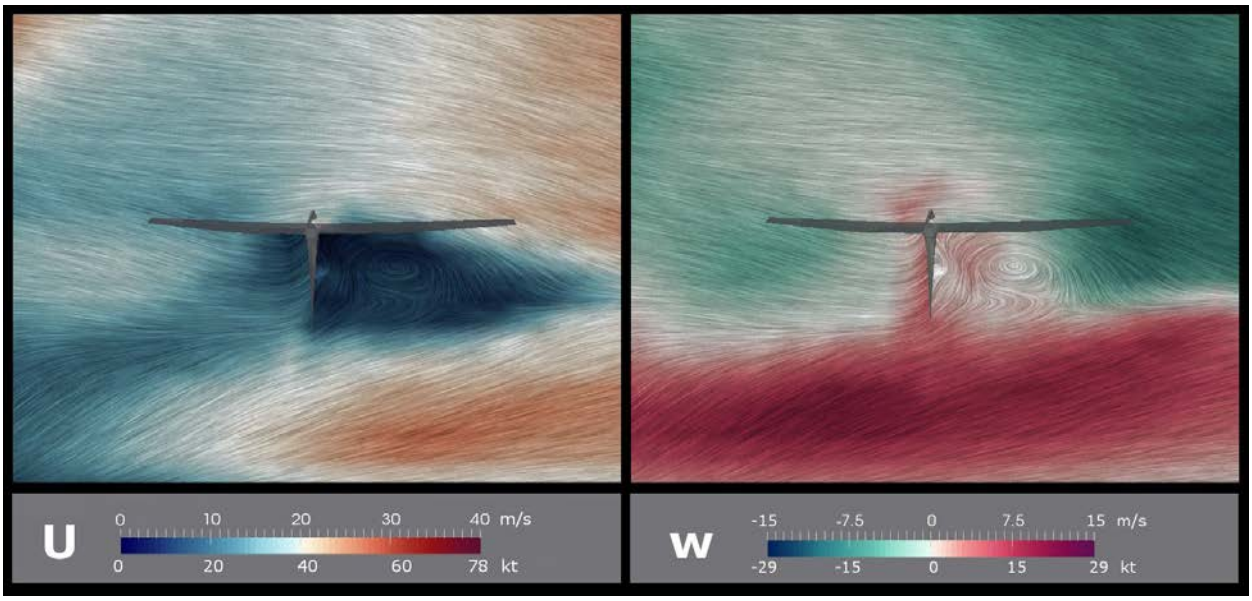

Figure 18. **U** and **w** for time = 34.9 sec.

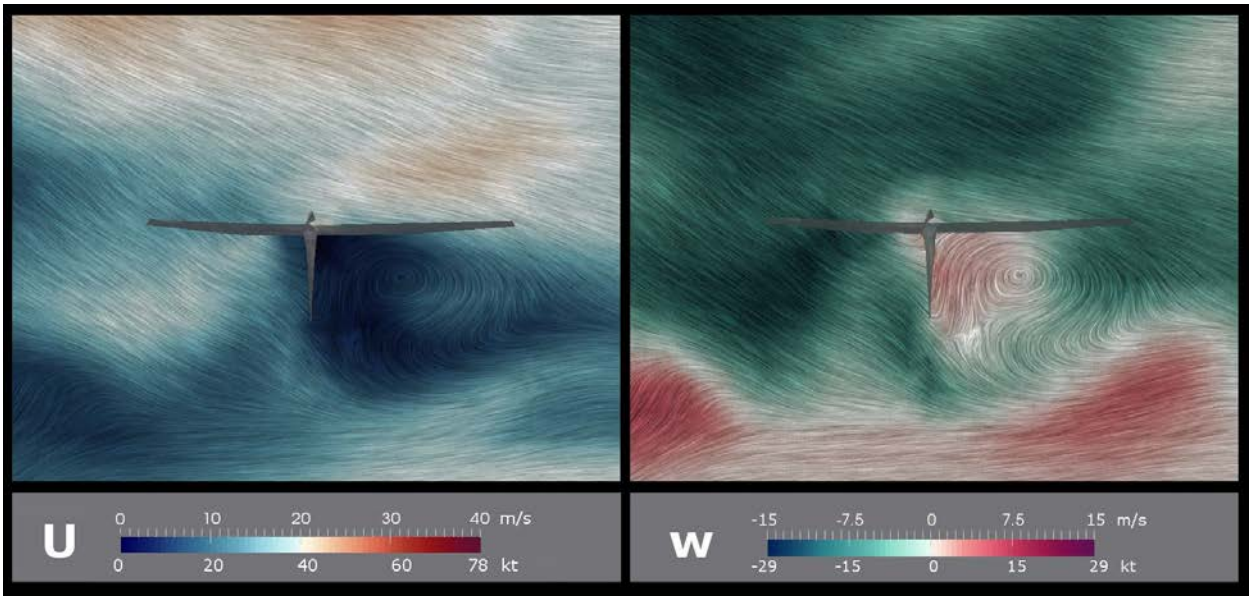

Figure 19. **U** and **w** for time = 35.6 sec.

During times 29-39 seconds of the model simulation, which relate to the maximum gusts recorded on ASOS, wind data at several locations (figure 20) were sampled from the model. These sampled wind data are shown in table 2.

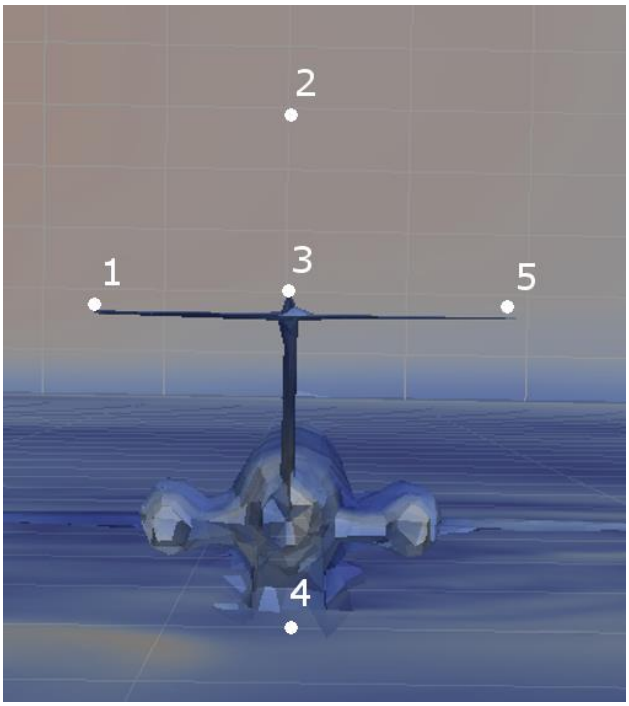

Figure 20. Point locations data were sampled during times 29-39 seconds.

	Point 1			Point 2			Point 3			Point 4			Point 5		
time sec	u	v	w	u	v	w	u	v	w	u	v	w	u	v	w
29.4	9.0	12.8	-11.1	18.1	-6.8	-9.1	6.0	8.9	-5.4	6.8	17.5	0.6	11.5	13.6	1.3
30.0	0.0	6.8	4.1	10.1	4.5	-12.1	11.1	-3.9	-1.1	10.1	16.9	-1.9	17.5	9.5	-3.3
30.7	1.9	5.1	-4.6	14.2	8.4	-9.9	1.8	2.7	-6.0	11.7	21.4	1.9	13.4	12.8	-7.6
31.2	8.0	17.6	-5.0	13.0	5.1	-12.6	5.4	5.4	-3.3	16.9	19.2	-0.6	18.9	12.2	-5.6
31.7	16.0	11.8	-7.6	25.3	7.8	-11.7	13.8	5.6	-2.7	18.5	15.6	-2.1	23.3	11.3	-6.8
32.2	31.1	16.6	-3.2	21.4	18.1	6.4	19.4	4.1	0.3	25.3	8.6	-1.1	29.2	15.6	-5.2
32.6	29.5	25.7	7.3	29.2	10.7	5.6	35.0	25.3	6.0	29.2	5.2	-0.9	40.8	21.4	-2.5
33.0	40.2	28.4	15.5	38.9	16.3	12.8	40.8	36.9	12.4	27.2	3.3	-1.6	38.9	33.0	2.9
33.4	38.3	19.6	15.7	36.9	21.4	21.4	42.8	35.0	25.3	27.2	7.2	0.1	44.7	35.0	12.2
33.8	37.7	1.1	7.3	52.5	-2.9	-2.7	42.8	25.3	12.4	33.0	18.7	3.5	40.8	15.2	7.2
34.1	48.8	-12.9	11.4	54.4	-0.3	-4.5	38.9	17.9	6.8	44.7	29.2	3.1	35.0	10.9	-4.5
34.5	25.9	-17.0	-1.1	46.7	-5.4	-9.1	44.7	-11.3	1.1	38.9	25.3	1.9	48.6	3.1	-9.5
34.9	25.3	-5.8	-6.6	35.0	2.1	-7.2	33.0	-7.2	-1.3	38.9	31.1	4.1	35.0	3.5	-5.8
35.3	20.0	-6.3	-6.6	29.2	-6.6	0.0	25.3	-10.9	-2.1	29.2	27.2	0.3	23.3	-0.8	-5.6
35.6	12.6	4.1	-8.0	23.3	10.1	-4.5	25.3	-13.6	-1.3	21.4	16.9	-3.1	21.4	1.0	-1.9
36.0	12.6	4.1	-8.0	16.7	14.8	-6.2	14.2	-1.9	-3.1	13.6	3.3	-3.3	11.9	3.5	-2.7
36.5	22.4	-3.5	0.2	18.9	18.1	1.5	12.4	6.0	1.8	9.7	-0.6	-1.4	17.7	0.9	-1.0
37.0	22.4	-3.5	0.2	17.3	9.9	2.7	13.6	0.2	-0.1	21.4	7.0	1.4	18.7	2.5	-2.7
37.5	15.5	-5.6	3.2	27.2	4.9	-2.1	23.3	1.1	1.9	25.3	7.0	-3.3	18.5	5.1	-3.9
38.0	25.3	-3.0	-0.7	36.9	-8.7	0.6	21.4	-0.5	2.7	25.3	-5.1	-1.1	16.1	7.2	-1.0
38.6	20.6	-15.6	4.7	31.1	-6.6	1.6	21.4	3.9	4.5	18.3	-5.8	0.0	16.7	6.6	-1.2
39.0	13.1	-1.9	5.5	25.3	12.8	0.3	23.3	-21.4	2.7	21.4	-7.0	0.5	13.4	5.6	2.5

Table 2. Tabular **u**, **v**, and **w** components (kt) for the points shown in figure 20.

Appendix I.

a. Selected Citations of Publications Utilizing OpenFoam

Mat Ali, Mohamed Sukri & Leong, L.L. & Ramly, M.N. & shaikh salim, sheikh ahmad zaki & Muhammad, S, 2017: Utilizing open source software running in inexpensive high performance computing system for cfd applications. *ARPN Journal of Engineering and Applied Sciences*, **12**, 3061-3067.

Ashvinkumar Chaudhari, Antti Hellsten, and Jari Hämäläinen, 2016: Full-Scale Experimental Validation of Large-Eddy Simulation of Wind Flows over Complex Terrain: The Bolund Hill. *Advances in Meteorology*, Article ID 9232759.

Chen, Goong & Gu, Cong & Morris, Philip & G. Paterson, Eric & Sergeev, Alexey & Wang, Yi-Ching & Wierzbicki, Tomasz, 2015: Malaysia Airlines Flight MH370: Water Entry of an Airliner. *Notices of the American Mathematical Society*, **62**, 330-344.

Daniele, Elia, 2017: Wind turbine control in computational fluid dynamics with OpenFOAM. *Wind Engineering*, **41**, 213-225.

Fragner, Moritz & Deiterding, Ralf, 2016: Investigating cross-wind stability of high-speed trains with large-scale parallel CFD. *International Journal of Computational Fluid Dynamics*, **30**, 402-407.

Han, Yi & Stöllinger, Michael & Naughton, Jonathan, 2016: Large eddy simulation for atmospheric boundary layer flow over flat and complex terrains. *Journal of Physics: Conference Series*, 753, 032044.

Jubayer, Chowdhury & Hangan, Horia, 2016: A numerical approach to the investigation of wind loading on an array of ground mounted solar photovoltaic (PV) panels. *Journal of Wind Engineering and Industrial Aerodynamics*, **153**, 60-70.

King, Marco-Felipe & L. Gough, Hannah & Halios, Christos & F. Barlow, Janet & Robertson, Adam & Hoxey, A & Noakes, Catherine, 2017: Investigating the influence of neighbouring structures on natural ventilation potential of a full-scale cubical building using time-dependent CFD. *Journal of Wind Engineering and Industrial Aerodynamics*, **169**, 265-279.

Lodh, Bibhab & Kumar Das, Ajoy & Singh, Navtej, 2017: Numerical Comparison of RANS and LES Turbulence Model for Wind Flow Over a Cube in a Turbulent Channel using OPENFOAM. International Journal of Engineering Research and Technology, **6**, 468-483.

Mendoza, Víctor & Goude, Anders, 2017: Wake Flow Simulation of a Vertical Axis Wind Turbine Under the Influence of Wind Shear. *Journal of Physics: Conference Series*, 854, 012031.

Niranjan S. Ghaisas & Cristina L. Archer, 2016: Geometry-Based Models for Studying the Effects of Wind Farm Layout. *Journal of Atmospheric and Oceanic Technology*, **33**, 481-501.

Sutherland, M & Etele, J & Fusina, G, 2016: Urban Wake-Field Generation Using Large-Eddy Simulation for Application to Quadrotor Flight. *Journal of Aircraft*, **53**, 1-13.

Urkiola, A & Fernandez-Gamiz, Unai & Errasti, I & Zulueta, Ekaitz, 2017: Computational characterization of the vortex generated by a Vortex Generator on a flat plate for different vane angles. *Aerospace Science and Technology*, **65**, 18-25.

Yijia Zheng, Yucong Miao, Shuhua Liu, Bicheng Chen, Hui Zheng, and Shu Wang, 2015: Simulating Flow and Dispersion by Using WRF-CFD Coupled Model in a Built-Up Area of Shenyang, China. *Advances in Meteorology*, Article ID 528618.

Yucong Miao, Shuhua Liu, Yijia Zheng, Shu Wang, and Yuan Li, 2014: Numerical Study of Traffic Pollutant Dispersion within Different Street Canyon Configurations. *Advances in Meteorology*, Article ID 458671.

Yu Cao, Xiao-Guang Ren, Xiao-Wei Guo, et al., 2015: A New Method to Simulate Free Surface Flows for Viscoelastic Fluid. *Advances in Materials Science and Engineering*, Article ID 159831.

Zhang, Ye & Sun, Zhengzhong & van Zuijlen, Alexander & van Bussel, Gerard, 2017: Numerical simulation of transitional flow on a wind turbine airfoil with RANS-based transition model. *Journal of Turbulence*, 1-20.

Zocca, Marta & Gori, Giulio & Guardone, Alberto, 2016: Blockage and Three-Dimensional Effects in Wind-Tunnel Testing of Ice Accretion over Wings. *Journal of Aircraft*, **54**, 1-9.

Appendix II.

Date	Time (EST)	Sustained Wind Dir	Sustained Wind (kt)	Gust Dir	Gust (kt)
20170308	1135	247	37	237	44
20170308	1136	245	38	240	47
20170308	**1137**	**243**	**41**	**240**	**47**
20170308	**1138**	**250**	**40**	**244**	**45**
20170308	**1139**	**257**	**39**	**261**	**55**
20170308	1140	255	36	254	42
20170308	1141	251	32	253	38
20170308	1142	248	32	244	41
20170308	1143	249	36	242	47
20170308	1144	251	38	249	42
20170308	1145	252	33	251	37